Available online at www.sciencedirect.com
ScienceDirect
Journal of the European Ceramic Society 30 (2010) 865–873
www.elsevier.com/locate/jeurceramsoc

Carbon nanotube toughened aluminium oxide nanocomposite

Iftikhar Ahmad [a], Hongzhi Cao [b], Huahui Chen [b], Huiyou Zhao [b], Andrew Kennedy [a], Yan Qiu Zhu [a,*]

[a] Division of Materials, Mechanics and Structure, Faculty of Engineering, University of Nottingham, University Park, NG7 2RD, UK
[b] Department of Materials Science and Engineering, China University of Mining and Technology, D11 Xueyuan Lu, Beijing 100083, China

Received 6 May 2009; received in revised form 21 September 2009; accepted 30 September 2009
Available online 25 October 2009

Abstract

This paper describes the mechanical properties of carbon nanotube-reinforced Al_2O_3 nanocomposites fabricated by hot-pressing. The results showed that compared with monolithic Al_2O_3 the fracture toughness, hardness and flexural strength of the nanocomposites were improved by 94%, 13% and 6.4% respectively, at 4 vol.% CNT additions. For 10 vol.% CNT additions, with the exception of the fracture toughness, which was improved by 66%, a decrease in mechanical properties was observed when compared with those for monolithic Al_2O_3. The toughening mechanism is discussed, which is due to the uniform dispersion of CNTs within the matrix, adequate densification, and proper CNT/matrix interfacial connections.

Keywords: Carbon nanotubes; Al_2O_3; Nanocomposite; Mechanical properties; Toughness

1. Introduction

Among ceramics, alumina (Al_2O_3) is the most widely used in material's industry and has potential applications covering high speed cutting tools, dental implants, chemical and electrical insulators, wear resistance parts and various coatings.[1,2] These applications arise from their high hardness, chemical inertness and high electrical and thermal insulation properties. However, low fracture toughness restricts this material from advanced structural applications, such as in aircraft engine parts, rocket materials surviving in extreme environments and numerous other space engineering applications.[3,4] The inferior fracture toughness of Al_2O_3 is attributed to the presence of impurities, pores and cracks formed during cooling after sintering; the elimination of such processing flaws in monolithic Al_2O_3 is extremely expensive and requires advanced processing technology. An alternative and practical way to convert Al_2O_3 into a more useful material is to fabricate a composite. Al_2O_3 can be reinforced with many materials ranging from metals such as Fe, Mo, Cr and Ni to ceramics such as ZrO, MgO, SiC and carbon fibres, and moderate improvements in fracture toughness have been reported.[5–13] Recent advances in nanotechnology have emerged along with numerous new nanomaterials possessing extraordinary properties. It is postulated that these nanomaterials could be incorporated into brittle ceramics to generate highly toughened composites that will be suitable for advanced engineering applications. Among nanomaterials, carbon nanotubes (CNTs) have attracted much attention due to their outstanding mechanical properties, very good electrical characteristics and excellent thermal performance. To date, CNT-reinforced Al_2O_3 nanocomposites have been reported and the resulting nanocomposites appeared to show wide variations in density, flexural strength, hardness and fracture toughness.[14,15] Consistently improved mechanical properties at low addition of CNTs (<4 vol.%) have been obtained, however wide scattered values for the fracture toughness are also observed, which is problematic when the CNT content is high (>4 vol.%).[16–18] This phenomenon was believed to have arisen from porosity in the composites, lack of uniformity in the CNTs dispersion, weak interfacial connections and possible damage to the CNTs.[19,20]

In this paper, the fabrication of CNT-reinforced Al_2O_3 nanocomposites consolidated by hot-pressing is demonstrated, along with systematic mechanical testing of the resulting composites. The aim is to show that Al_2O_3–CNT nanocomposites can be potential candidates for advanced engineering applications.

* Corresponding author.
E-mail address: Yanqiu.zhu@nottingham.ac.uk (Y.Q. Zhu).

0955-2219/$ – see front matter.
doi:10.1016/j.jeurceramsoc.2009.09.032

2. Experimental procedure

2.1. Materials and fabrication

Multi-walled CNTs (∅ ∼ 40 nm, Tsinghua University, Beijing, China) were well-dispersed in distilled water by the combined actions of utilising ultra-sonication, adding surfactant and choosing suitable incubation time. For example, 0.1 g of hot nitric acid-treated CNTs were added into 100 ml of distilled water in a beaker containing a small amount of sodium dodecyl sulphate (SDS, 1–2 wt.% of the CNT) surfactant and processed for 30 min using an ultrasonic probe (Sonic processor D-100-20, manufactured by Sonic system, UK, using a power of 30–40 W). The probe sonication can break the large bundles in to small ones, so that the surfactant can be easily adsorbed onto the CNT surfaces. The sonication duration was optimised by visual observation of the CNT bundles in distilled water and it was observed that short sonication process time (<30 min) led to inadequate breakage of CNT bundles and few large bundles were found at the bottom of the beaker. Increasing the sonication time (>30 min) did not reveal any significant difference in the size of CNT bundles in distilled water. The CNT/distilled water suspension was then incubated, at ambient conditions, for 2–6 weeks to allow a thorough surfactant adsorption onto the CNT surfaces, to effectively counter the Van der Waals interactions. After re-sonication, detangled and relatively stable CNT suspensions in distilled water was obtained.[21] 5 g δ-Al_2O_3 nanoparticles (∅ < 40 nm, Sigma–Aldrich, UK) were then added into the CNT/water suspension, for 4 vol.% CNT composites. Sonication was again applied for 120 min. The mixture was dried using a hot plate at 120–150 °C under sonication until a slurry was formed and no further sonicating effect was observed. After milling in a mortar, the mixed powder was then consolidated by hot-pressing in a graphite die (University of Mining and Technology, Beijing, China) under a pressure of 40 MPa at 1600 °C for 60 min, at a heating rate of 10 °C/min, under vacuum (6.2×10^{-2} Pa). ∅ 32 mm × 3 mm discs of nanocomposites with different CNT contents were produced. Monolithic Al_2O_3 was also hot-pressed under identical experimental conditions for comparison.

2.2. Structural characterisation

Structural features of the fractured samples were assessed using scanning electron microscopy (SEM), and images were acquired using secondary electron (SE) signals. Prior to SEM observation, the samples were gold coated for 1 min. X-ray diffraction (XRD, Siemens D500 and Bruker D8 Advanced X-ray Diffractometer, using Cu k_α radiation) was utilised to identify the crystalline phase features of the nanocomposites, with the assistance of computer software (DIFFRAC^{plus} and by Bruker Advanced X-ray Solutions). SEM and XRD techniques were also employed to determine the sample grain sizes. To reveal the grain boundaries, for grain size determination using SEM, samples were thermally etched for 15 min at 1400 °C under an Ar atmosphere in a tube furnace. Prior to etching, all samples were polished up to 1 μm using diamond paste. Transmission electron microscopy (TEM, JEOL 2000 FX and 2100 F) was used to characterise the interface structures of the nanocomposites. Two methods, chemical etching and FIB/SEM milling, were adopted to prepare samples for TEM analysis. In chemical etching method, samples were prepared by deep etching small pieces of the composites using NaOH for 2 weeks followed by a thorough rinsing with distilled water in order to remove traces of NaOH and recover the desired samples. The clean samples were dispersed in acetone and then transferred onto a holey carbon film, supported on a copper grid, for observation. In FIB-SEM (FEI Quanta200 3D DualBeam FIB/SEM) sample preparation technique, the surrounding area of the desired section of the nanocomposite sample was removed by the bombardment of Ge-ions. Subsequently, the milled section was carefully detached from the bulk sample by welding it with a special probe for further TEM analysis. Both techniques produced good quality Al_2O_3–CNT nanocomposite thin samples suitable for TEM investigations.

2.3. Properties evaluation

Archimedes method was employed to measure the densities of the discs (using distilled water), and the relative densities were calculated by dividing the apparent density by the theoretical density. In this study, 3.97 g/cm^3 and 1.85 g/cm^3 were used as theoretical densities for Al_2O_3 and CNTs, respectively.[20,22] Microhardness testing was carried out at 9.8 N loads for 15 s (M-400 hardness tester, LECO, Japan). The diagonal lengths of the indents were measured using the attached microscope, converted to Vickers hardness number (HV) and further converted to GPa.[13] The flexural strength (σ_f) was measured in three-point bending, in which the specimen size was 25 ± 1.5 mm (length) × 2 ± 0.15 mm (breath) × 2.5 ± 0.20 mm (height). The bending span and the testing speed for the test were 20 mm/min and 0.50 mm/min respectively, and flexural strength was assessed using Eq. (1):[23]

$$\sigma_f = \frac{3FL}{2bd^2} \tag{1}$$

where F is the load at the fracture point, L is the span length, b is the sample breath and d is the sample thickness.

The fracture toughness (K_{IC}) was evaluated using the direct crack measurement (DCM), indentation strength in bending (ISB) and single edge notched beam (SENB) methods. In the DCM method, the fracture toughness was obtained by applying Eq. (2):[24]

$$K_{IC} = 0.016\left(\frac{E}{H}\right)^{1/2}\left(\frac{P}{c^{3/2}}\right) \tag{2}$$

where E is the modulus of elasticity, H is the hardness and c the radial crack length generated by Vickers's indentation. The crack length was measured from the indentation centre using scanning electron microscopy, SEM, (Philips/FEI XL30-JEOL 6400; Philips/FEI XL30 FEG-ESEM), in combination with computer software ImageJ (Image Processing and Analysis in Java).

The indentation strength in bending (ISB) method was also used to evaluate the fracture toughness. In the ISB method, three

samples were prepared with identical dimensions using similar processes for preparing the flexural strength testing specimens. In this case, an indent was made at the middle of the sample using a hardness tester with a diamond Vickers indenter using a load of 10 kg (98 N). This load was carefully selected to ensure that the crack size was above the critical size, in order to obtain meaningful results. During three-point bending, all samples broke exactly at where the indent was made. The fracture toughness was thus calculated using Eq. (3):[25]

$$K_{IC} = 0.59\left(\frac{E}{H}\right)^{1/8}(\sigma P^{1/3})^{3/4} \quad (3)$$

where E is the Young's modulus, H is the hardness, σ the flexural strength in the presence of the Vickers indent and P the load at failure.

For SENB method, three notched samples were prepared with identical dimensions. The ratio of the notch depth to specimen height is a/W ~0.45–0.55. Three-point bent tests were performed at a loading speed of 0.05 mm/min. The fracture toughness was calculated using the following Eq. (4):[26]

$$K_{IC} = \frac{3P_{max}L}{2BW^{3/2}}\alpha^{1/2}Y \quad (4)$$

where P is the breaking load during three-point bending test, L is the bending span, B is the specimen breath, W the specimen height and a is the notch depth, α is the ratio between a and W, and Y is the calibration factor which was calculated by Eq. (5), given below:[26]

$$Y = \frac{1.99 - \alpha(1-\alpha)(2.15 - 3.93\alpha + 2.7\alpha^2)}{(1+2\alpha)(1-\alpha)^{3/2}} \quad (5)$$

A standard ultrasonic pulse-echo technique was used to assess the modulus of elasticity of monolithic Al_2O_3 and the Al_2O_3–CNT nanocomposites. During the pulse-echo measurements, the time-of-flight velocities for both compression and shear wave propagation through the samples were recorded. Compression measurements were made using 20 MHz centre frequency, ∅ 6 mm contact transducers (TMP-3, Sonatest, UK). The equivalent shear measurements were performed with a 10 MHz centre frequency, ∅ 10 mm contact transducer (V221-BA, Panametrics, USA). Appropriate couplant materials were used in each case to ensure optimum contact between the samples and transducers. From the velocity measurements, the modulus of elasticity for monolithic Al_2O_3 and Al_2O_3–CNTs nanocomposites were calculated by employing Eq. (6):[27]

$$E = \frac{V_s^2\rho(3V_c^2 - 4V_s^2)}{V_c^2 - V_s^2} \quad (6)$$

where E is the Young's modulus, ρ is the bulk density of the samples, V_c is the compression velocity and V_s the shear velocity.

3. Results

Fractographic details of the nanocomposite reinforced with 4 vol.% of CNTs revealed the well-dispersed CNTs within the Al_2O_3 matrix (Fig. 1a). At higher magnification (Fig. 1b), the individually dispersed CNTs are clearly visible. At higher CNT additions (10 vol.%), a few CNT bundles were also observed, as black arrowed in Fig. 1c. The CNT contents affected the sintered densities of the nanocomposites, as summarised in Fig. 2. 99.7% relative density for monolithic Al_2O_3 was obtained, however 0.5% and 3.4% reductions were resulted for nanocomposites containing 4 and 10 vol.% CNTs, respectively.

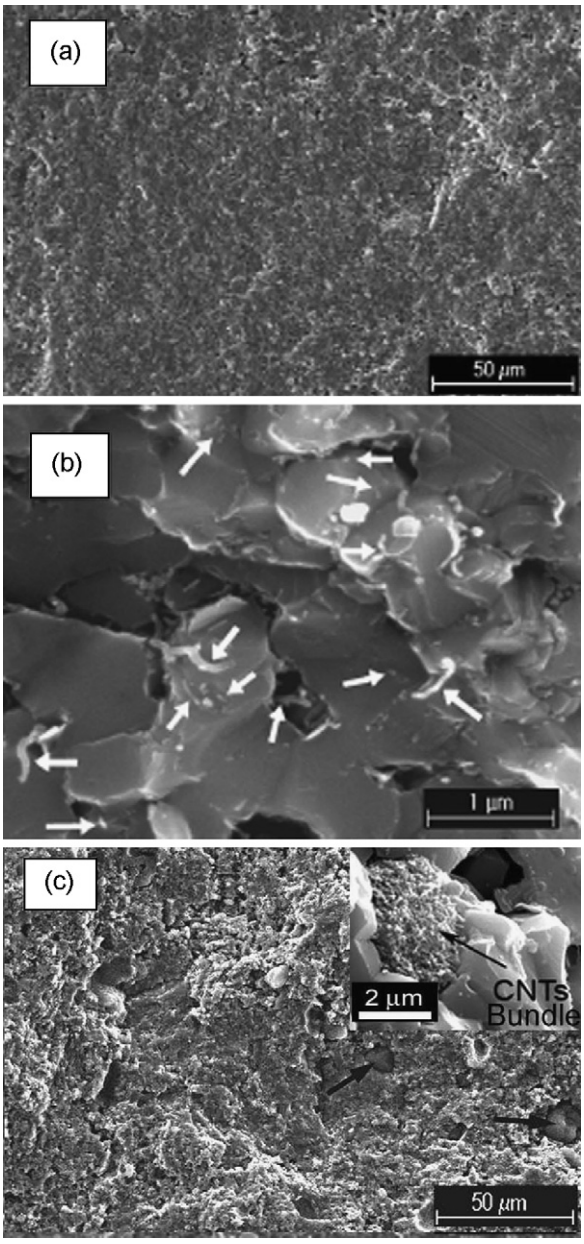

Fig. 1. SEM images showing the dispersion of 4 vol.% CNTs in Al_2O_3. (a) Low magnification, (b) higher magnification (white arrows show CNTs), and (c) blocks of CNT (black arrowed) in nanocomposite at 10 vol.% CNT concentration, and the inset shows the CNT agglomerate.

Phase analysis using XRD exhibited the typical peaks of crystalline α-Al_2O_3 (JCPDS No. 01-078-2426) for the sintered monolithic Al_2O_3, and graphite peaks (JCPDS No. 01-075-1621) for pure CNTs, as shown in Fig. 3a and b. However, their nanocomposites showed only peaks of crystalline α-Al_2O_3, and no obvious peaks associated with CNTs are observed, as shown

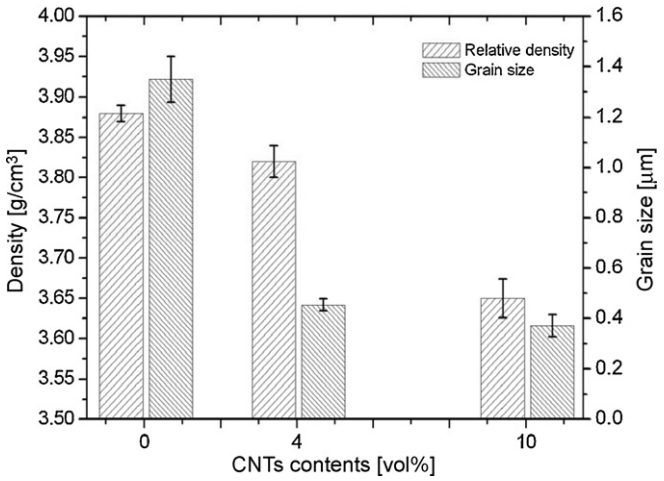

Fig. 2. Density and grain size of Al_2O_3 matrix as a function of CNT addition.

in Fig. 3c and d. Due to the low CNT contents in nanocomposites and the low X-rays diffraction density of CNTs compared with the highly crystalline Al_2O_3, the (0 0 2) peak of the CNT was masked.

Structural features of the fractured and thermally etched surfaces of the samples were observed using SEM. Fig. 4a shows large and uneven grains for the monolithic Al_2O_3 however the composites exhibited a sharp decrease in the grain size, by 66% at 4 vol.% CNTs and 75% at 10 vol.% CNTs, in comparison to the monolithic Al_2O_3, as demonstrated in Fig. 4b and c, and summarised in Fig. 2. Close inspection of the thermally etched nanocomposite samples revealed interesting features, conventional depression/negative curvature of grain boundary was observed for monolithic Al_2O_3 (Fig. 4a), as expected, however entirely new structural features were found in nanocomposites samples where the Al_2O_3 grains appear to be etched away, leaving the grain boundaries sticking out, as displayed in Fig. 4b and c. In addition to altering the grain size, the existence of CNTs also effectively modified the mode of matrix fracture, from inter-granular fracture (Fig. 5a) for monolithic Al_2O_3, to trans-granular fracture in the nanocomposites, as exhibited in Fig. 5b and c.

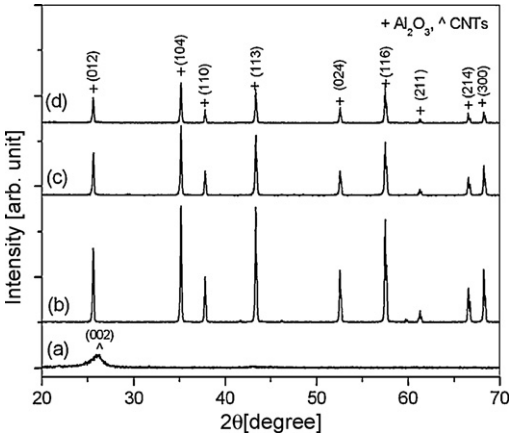

Fig. 3. XRD patterns. CNTs (a), and Al_2O_3–CNT nanocomposites containing: (b) 0 vol.%, (c) 4 vol.% and (d) 10 vol.% CNTs.

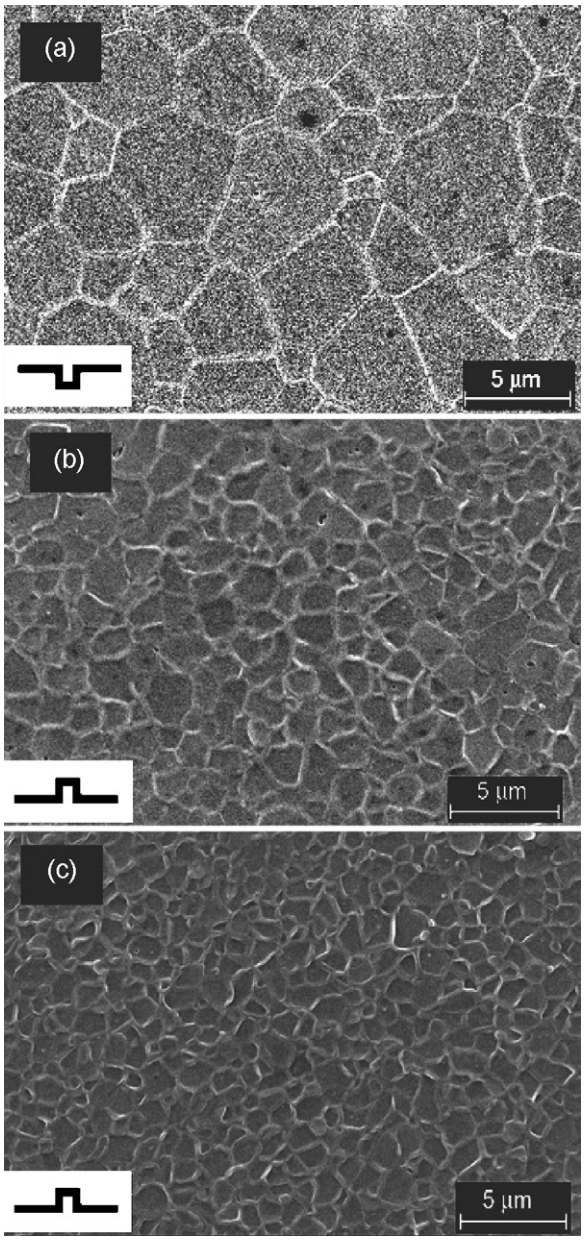

Fig. 4. Thermally etched surfaces of sintered (a) monolithic Al_2O_3 showing negative curvature or depressed grain boundary; (b) 4 vol.% CNT and (c) 10 vol.% CNT nanocomposites both exhibiting a positive curvature at grain boundaries. Insets illustrating the grain boundary type.

The fracture toughness obtained by the SENB method showed 94% and 66% improvement for 4 and 10 vol.% CNT additions respectively, when compared with the monolithic Al_2O_3 (Fig. 6). The results obtained by using the DCM and ISB methods were also displayed in Fig. 6, which improved by 42% and 47% for the DCM technique, and by 32% and 35% for the ISB method, for the same 4 vol.% and 10 vol.% CNT composites, respectively. Marginal 12% and 6% increases in hardness and flexural strength were also obtained for composite with 4 vol.% CNT addition. However, a small reduction of 7% in hardness and a significant drop (21%) in flexural strength were recorded with 10 vol.% CNT addition, as shown in Fig. 7.

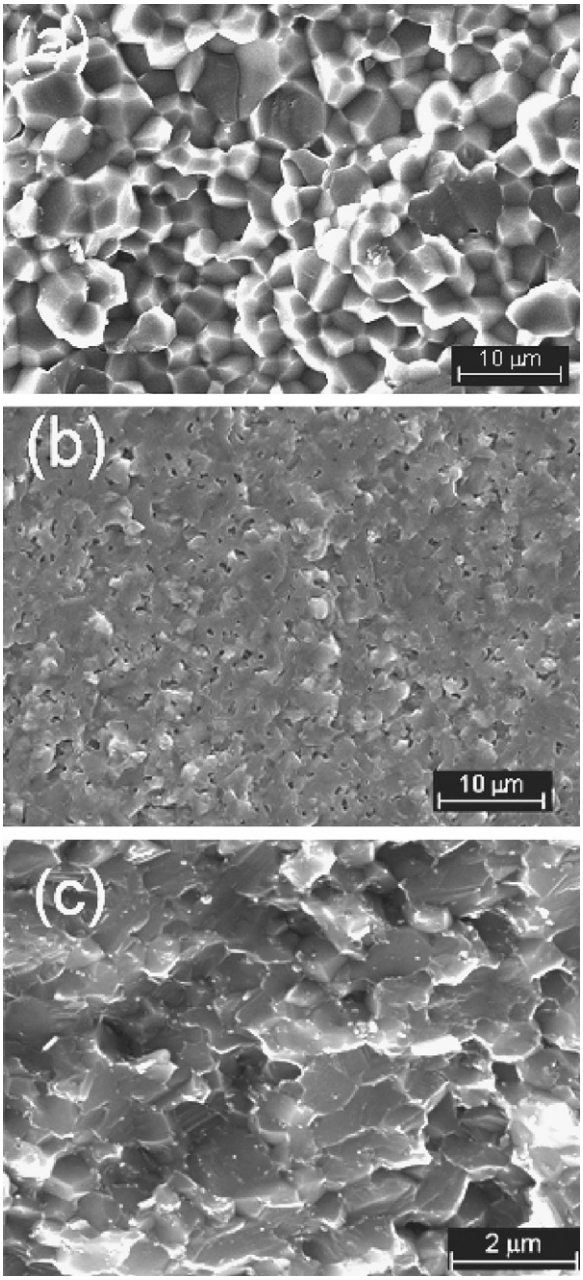

Fig. 5. SEM fractured surface images. (a) Monolithic Al_2O_3 indicating intergranular fracture; (b) Al_2O_3–CNT 4 vol.% nanocomposites exhibiting transgranular fracture at low magnification, and (c) high magnification of (b).

4. Discussions

4.1. Structural features

Obtaining high theoretical densities is important for producing nanocomposites with good mechanical properties.[17,21,28] Well-dispersed CNTs in a matrix lead to higher sintered densities, whilst agglomerates result in lower densities. In this context, successful dispersion of CNTs within the Al_2O_3 matrix was obtained. After hot-pressing, the SEM images of the fractured composite surfaces have revealed the well-dispersed CNTs within the matrix (Fig. 1a and b) at 4 vol.%, however a few small bundles elucidate the difficulties of CNT dispersion at higher CNT volume. The abrupt decrease in grain size at low CNT addition (4 vol.%) is associated with the grain boundary pinning phenomenon caused by CNTs, due to their tendency to accumulate at grain boundaries during sintering process, as shown in Fig. 4b. Furthermore, raising the CNT content up to 10 vol.% has a main effect of merely increasing the concentration of CNTs at the grain boundaries, rather than significantly increasing the number of boundaries being pinned, thus only a 14% further decrease in the grain size was observed, as displayed in Figs. 2 and 4c.[31]

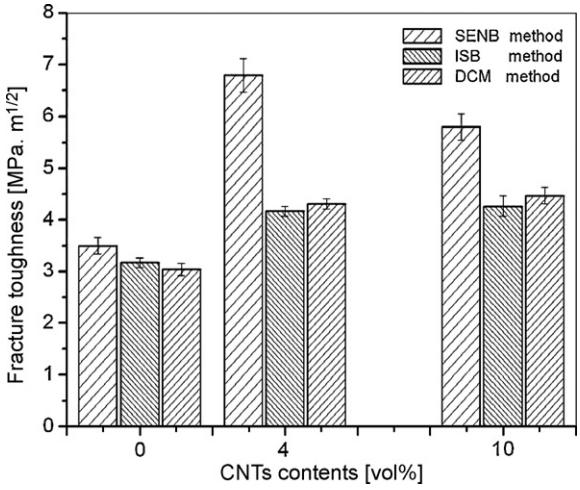

Fig. 6. Fracture toughness of Al_2O_3–CNT nanocomposites obtained by different methods, with different CNT additions.

4.2. Mechanical properties

4.2.1. Fracture toughness

Both the DCM and ISB methods are well-established techniques which were widely used in numerous reports.[18,28,29] However, they have been challenged recently and are considered less reliable than the SENB method for assessing the fracture toughness of ceramics due to the three dimensional complexity

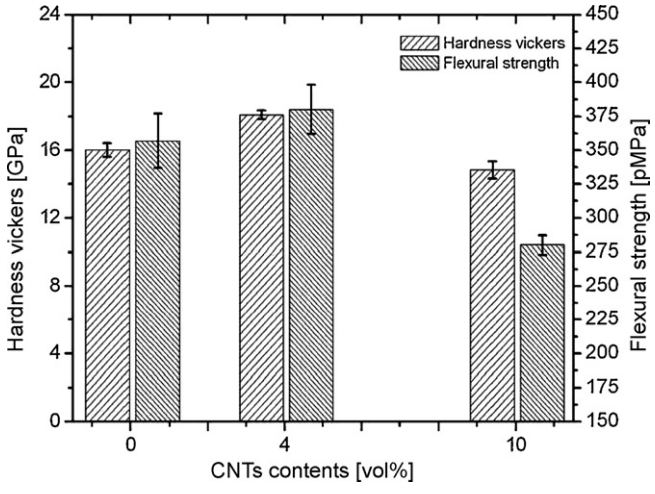

Fig. 7. Hardness and flexural strength of Al_2O_3 as function of CNT additions.

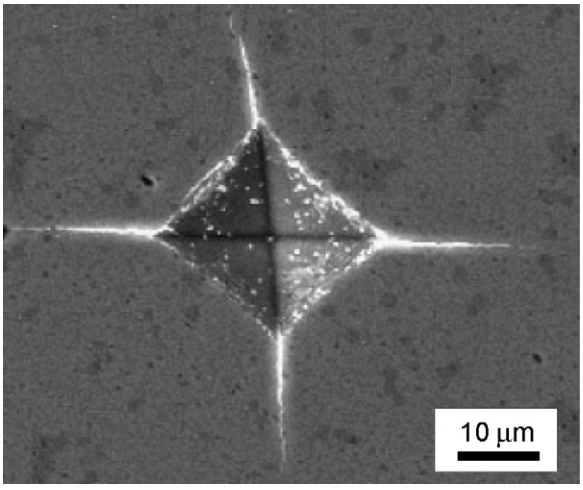

Fig. 8. SEM image of Vickers hardness indent cracks of Al_2O_3–CNT 4 vol.% nanocomposites at 9.8 N.

of indent cracks (Fig. 8), and possible surface damage that can occur around the indent cracks.[30] Therefore, in this context, the results obtained by employing the standard SENB method have been compared with those obtained in similar studies. Table 1 summarises the fracture toughness results obtained using the SENB method in this study, in comparison with data from literatures concerning the Al_2O_3–CNT nanocomposites, along with other process parameters associated with CNT dispersion and consolidation.

In previous studies, Table 1, the CNT dispersion was mainly relied on surfactant characteristics, however in this study prolonged reaction time was introduced which allowed surfactant to thoroughly adsorb on the CNTs which led to CNTs dispersed well within Al_2O_3 matrix. This could lead to higher fracture toughness for the nanocomposites.[14–20] Indeed, the higher fracture toughness values obtained in this study are believed to be due to the improved dispersion of CNTs with matrix, which was achieved by adopting combined method.

CNTs/matrix interactions are other important factors in explaining the improvement in toughness. TEM studies disclose various features of the CNT–Al_2O_3 interaction. It can be seen that a CNT was attached to three grains at the junctions as shown in Fig. 9a, thus it is possible to strengthen the grain boundaries of nanocomposites. This suggestion of grain boundary strengthening is evidenced by the change of fracture mode in nanocomposites because trans-granular fracture dominates only when the strength of the grain boundary is close to that of the matrix grain.[31] Strongly bonded CNTs make the matrix fracture through the grains rather than along grain boundaries, as prevails in monolithic Al_2O_3.

Conventional toughening mechanism for fibre-reinforced composites includes fibre pull-out and crack bridging. In this context, it is observed that CNTs formed bridges across the Al_2O_3 grains or gaps (arising from porosity and other processing defects), as displayed in Fig. 9b. Further SEM images (Fig. 10Ab and Bb) clearly demonstrate such bridging features of CNTs, indicating a potential crack bridge toughening mechanism. CNTs exist at the junction of grains (Fig. 10Ea), exhibiting

Table 1
Comparison of fracture toughness results with previously reported CNTs reinforced Al_2O_3 nanocomposites.

CNTs contents (vol.%)	Ref. 14 (Fan et al.)		Ref. 15 (Yamamoto et al.)	Ref. 16 (Laurent et al.)	Ref. 17 (Jinpeng et al.)	Ref. 18 (Zhan et al.)	Ref. 19 (Siegel et al.)	Ref. 20 (Wie et al.)	Present study
	CNTs and UT	CNTs + UT + SDS	CNTs (AT) and UT	Chemically grown Al_2O_3–CNTs–Fe composite powder	Hetero-coagulation process using SDS surfactant	UT mixing of Al_2O_3–CNTs in ethanol	UT mixing of Al_2O_3–CNTs	CNTs + UT + SDS	CNT + water + UT + SDS+ suitable storage of CNTs containing SDS and then mixed with Al_2O_3
	HP	HP	HP	HP	HP	SPS	HP	HP	HP
	SENB	SENB	SENB	SENB	SENB	SENB	DCM	SENB	SENB
0	3.08	3.08	4.4	4.4	3.3	3.3	3.4	2.8	3.50
1			5.9		5.12				
2			5.7		6.40				
3								5.0	
4			4.5	4.5					6.79
5								3.8	
6						7.9			
10	3.26	5.5		5.0		6.4	4.2		5.80

UT: ultrasonic stirring; SENB: single edge notch beam; AT: acid treated; DCM: direct crack measurement; SDS: sodium dodecyl sulphate, a surfactant; ISB: indent strength beam; SPS: spark plasma sintering; HP: hot-pressing.

pull-out features during crack propagation. Thus, it is believed that the conventional toughening mechanism is still applicable to the composites.

However, with regard to the energy absorbing role of CNTs during pull-out, the friction forces at the nanoscale is much more complicated than those produced in conventional micro-sized fibre-reinforced composites. CNTs that are located within the matrix grains demonstrate new features for the toughening mechanism. During crack propagation, the CNTs can be elastically deformed whilst keeping both tube ends firmly attached to the base grains (Fig. 10Eb) because CNT can sustain 40% strain before fracture.[32] In extreme cases, collapse or fracture of the CNT may occur (Fig. 10Ec) during the course of crack propagation when the deformation of nanocomposites exceeds the maximum strains of the CNT. Nevertheless, the CNT must have undergone large deformations, and owing to the high elastic modulus (>1 TPa) and extraordinary flexibility,[33,34] they absorbed significant amounts of energy which is associated with the work done by the elastic extension of CNTs over a distance at either side of the fractured surfaces, before collapse or fracture. Hence, CNTs indeed contributed to the improvement in toughness via an energy dissipation mechanism. Fig. 10C and D shows a broken CNT firmly attached to the matrix grain, providing evidence for such a mechanism.

The toughening effect strongly depends on the interfacial connection of CNTs with matrix. High-resolution TEM images shown in Fig. 9c display the firm attachment of CNTs to the matrix. We have previously reported that in the presence of a reducing atmosphere and at elevated temperatures, Al_2O_3 underwent a carbothermal reduction in the presence of CNTs, and formed an interfacial oxycarbide (Al_2OC) layer at the Al_2O_3/CNTs interface.[35] This layer presumably has a high chemically compatibility with both the CNT and the matrix, which has the capability to transfer loads effectively from the matrix to CNT and vice versa. With such strong interfacial connections, the matrix holds the CNTs firmly and the intrinsically high elastic properties of CNTs become functional, leading to increased toughness for the composites. The positive curvatures of grain boundaries in nanocomposites samples, Fig. 4b and c, can be considered as an indirect evidence for the presence of the possible new interfacial phase between the CNT and matrix.[35] Such features negate the impression of the oxidation of CNTs during thermal etching, however the preferential thermal etching of matrix indicates that the new phase formed at grain boundary around some of outer surfaces of CNTs is much more thermally stable, in comparison to the Al_2O_3 matrix.

The repression of nanocomposite fracture toughness (15%) at higher CNT concentration (10 vol.%), when compare with 4 vol.% CNT addition, is primarily due to the presence of sub-agglomerates of CNTs (Fig. 1c), underlining the complications for achieving homogenous dispersion of CNTs at higher concentrations which have been discussed in various reports.[20,21] Furthermore, being high in volume in the matrix, CNTs preferably accumulated at grain boundaries and strongly inhibited the diffusion mechanism, resulting in depressed density (Fig. 2) and weak interfacial connection between CNTs agglomerates

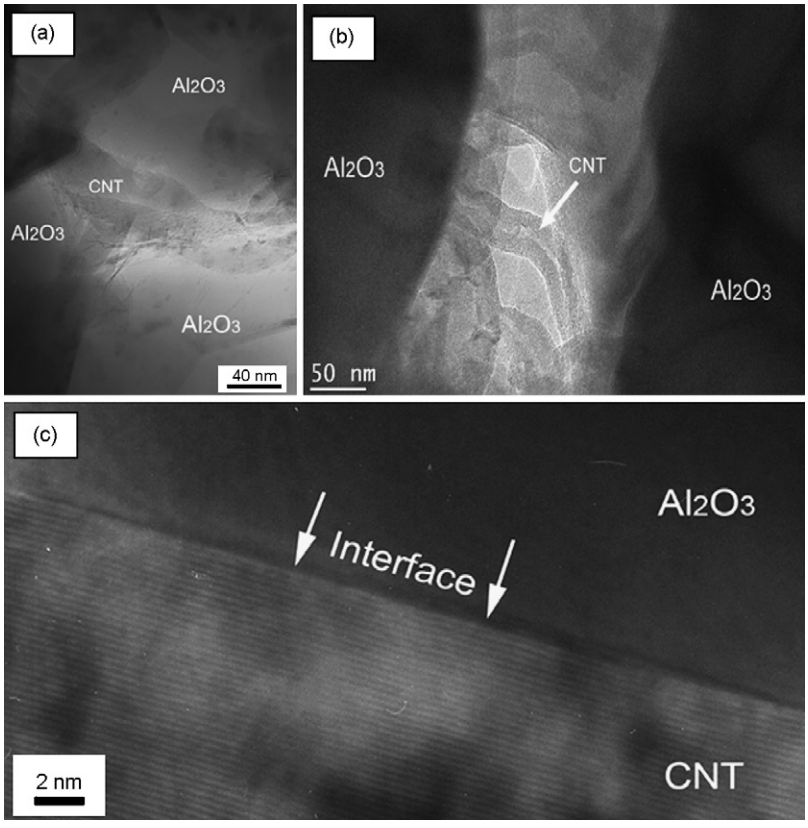

Fig. 9. (a and b) TEM image Al_2O_3–CNT nanocomposites showing locations of the CNT, and (c) high-resolution TEM image showing the interface of the Al_2O_3–CNT (arrowed).

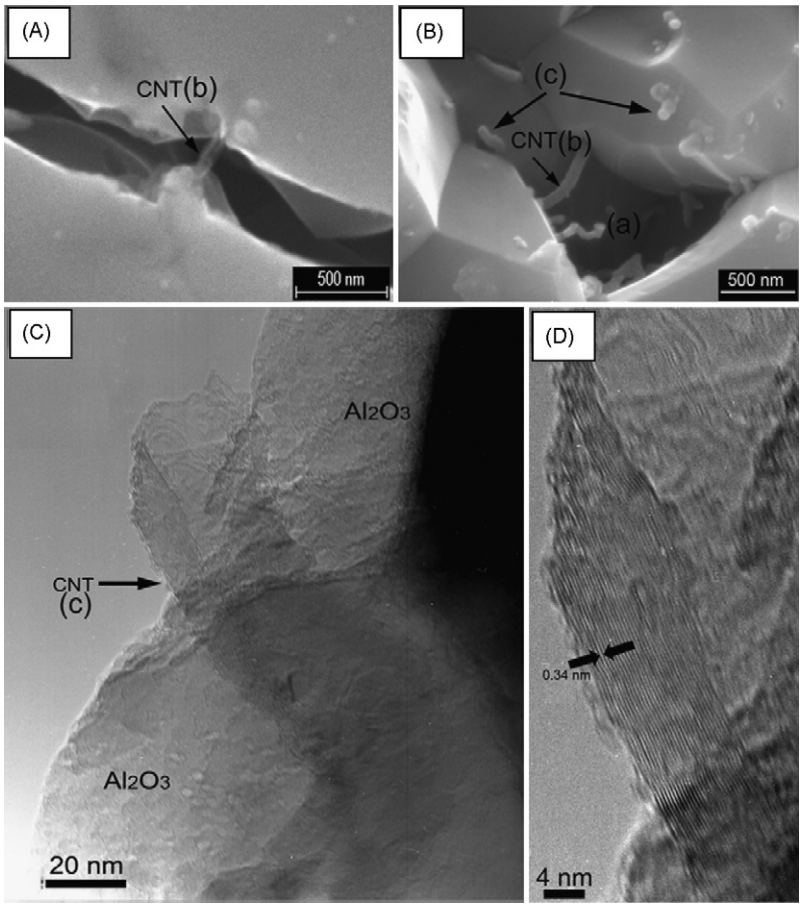

Fig. 10. SEM images of Al_2O_3–CNT nanocomposites (A) b—crack bridging phenomenon, (B) a—CNT pull-out, b—crack bridging and c—broken CNT; TEM images of (C) c—broken CNT and (D) high-resolution TEM images of the broken CNT.

and matrix.[16] Thus, these possible the toughening mechanisms are not fully operative, resulting in a slightly reduced fracture toughness.

4.2.2. Other mechanical properties

CNTs also enhanced other mechanical properties of the nanocomposites, such as hardness and flexural strength (Fig. 7). In this context, the increases in hardness and flexural strengths at low CNT addition are again associated with the strong connections of the well-dispersed CNTs with the matrix, which resulted in effective load transfer from the matrix to the CNTs. However, a negligible improvement in stiffness at low CNT additions, followed by a significant drop at high CNT contents can be attributed to adverse effects associated with poor densification of the nanocomposites. Since CNTs hampered the densification process, inhibited the grain growth, more elongated pores existed in the composite, as has been reported by many other groups.[36,37] This could be responsible for the lower flexural strength in nanocomposites.

5. Conclusions

The additions of CNT exhibited a strong influence over the grain size, density, fracture mode and overall mechanical properties of Al_2O_3–CNT nanocomposites. Conventional hot-pressing is an effective technique for achieving high performance ceramic nanocomposites at low CNT addition. A significant improvement of 94% in fracture toughness at 4 vol.% CNT concentration has been obtained, which is slightly decreased to 66% when increasing the CNT content to 10 vol.%. The toughening mechanism operative in the nanocomposite was discussed. It is believed that both the conventional fracture toughening mechanism (pull-out and crack bridging) and CNT energy dissipation mechanism via elastic deformation played their part in the nanocomposites.

Acknowledgements

IA is highly grateful to the Government of Pakistan and The University of Nottingham for the scholarship support. YZ thanks Mr K Dinsdale and Mr T Buss for their technical support.

References

1. Osayande, L. and Okoli, O. I., Fracture toughness enhancement for alumina system: a review. *Int. J. App. Ceram. Technol.*, 2008, **5**(3), 313–323.
2. Wu, Y., Zhang, X. and Guo, J., Microstructural development and mechanical properties of self-reinforced alumina with CAS addition. *J. Eur. Ceram. Soc.*, 2001, **21**, 581–587.
3. Ohnabe, H., Masaki, S. and Sasa, T., Potential application of ceramics matrix composites to aero-engine components. *Composites: Part A*, 1999, **30**, 489–496.

4. Miyazaki, H., Yoshizawa, Y. and Hirao, Preparation and mechanical properties of 10 vol% zirconia/alumina composite with fine scale fibrous microstructure by co-extrusion process. *Matter. Lett.*, 2004, **58**, 1410–1414.
5. Trusty, P. A. and Yeomans, J. A., The toughness of alumina with iron: effects of iron distribution on fracture toughness. *J. Eur. Ceram. Soc.*, 1997, **17**, 495–504.
6. Wie, W. and Cheng, F., Characterization of Al_2O_3 composites with fine Mo particulates, I: microstructural development. *Nanostruct. Mater.*, 1998, **10**(6), 965–981.
7. Marcin, C. and Katarzyna, P., Processing and mechanical properties of Al_2O_3–Cr nanocomposites. *J. Eur. Ceram. Soc.*, 2007, **27**, 1273–1279.
8. Yaoa, Y., Michel, D. I., Mazerolles, L. and Pastol, J., Alumina–nickel composites densified by spark plasma sintering. *Matter. Lett.*, 2005, **59**, 2314–2318.
9. Dogam, C. P. and Hawk, J. A., Role of zirconia toughening in abrasive wear of intermetallic and ceramics composites. *Wear*, 1997, **212**, 110–118.
10. Chakravarty, D. and Sundaresan, R., Spark plasma sintering of magnesia-doped alumina with high hardness and fracture toughness. *J. Am. Ceram. Soc.*, 2008, **91**(1), 203–208.
11. Carroll, L. and Derby, B., Silicon carbide particles size effects in alumina based nanocomposites. *Acta Mater.*, 1996, **44**(11), 4543–45552.
12. Jung, W. and Kwon, J., Penetration mechanics of ceramics composites armour made of alumina/GFRP. *Int. J. Prec. Eng. Manuf.*, 2007, **8**(4), 38–44.
13. Maensiri, S. and Amornkitbamrung, V., Carbon nanofiber-reinforced alumina nanocomposite: fabrication and mechanical properties. *J. Mater. Sci. Eng.*, 2007, **A477**, 44–50.
14. Fan, J., Zhao, D. and Song, J., Preparation and microstructure of multi-walled carbon nanotubes toughened Al_2O_3 composite. *J. Am. Ceram. Soc.*, 2006, **89**(2), 750–753.
15. Yamamoto, G., Omori, M., Hashida, T. and Kimura, H., A novel structure for carbon nanotube reinforced alumina composites with improved mechanical properties. *Nanotechnology*, 2008, **19**, 315708.
16. Laurent, C., Peigney, A. and Rousset, A., Carbon nanotubes–Fe–alumina nanocomposites. Part II: microstructure and mechanical properties of the hot-pressed composites. *J. Eur. Ceram. Soc.*, 1998, **18**, 2005–2013.
17. Jinpeng, F., Zhao, D. and Song, J., Preparation and microstructure of multi-walled carbon nanotubes-toughened Al_2O_3 composites. *J. Am. Ceram. Soc.*, 2006, **89**(2), 750–753.
18. Zhan, G., Kuntz, J., Wan, J. and Mukherjee, K., Single walled carbon nanotubes as attractive toughing agent in alumina based nanocomposites. *Nat. Mater.*, 2003, **2**, 38–42.
19. Siegel, R. W., Chang, S. K., Ajayan, P. M. and Schadler, Mechanical behaviour of polymer and ceramic matrix nanocomposite. *Scripta Mater.*, 2001, **44**, 2061–2064.
20. Wie, T., Fan, Z. and Wie, F., A new structure for multi-walled carbon nanotubes reinforced alumina nanocomposite with high strength and toughness. *Mater. Lett.*, 2008, **62**, 641–644.
21. Ahmad, I., Kennedy, A. and Zhu, Y. Q., Carbon nanotubes-reinforcing MgO-doped Al_2O_3 nanocomposites. In *Proceedings of the ECCM13: 13th European Conference on Composite Materials*, 2008.
22. Ajayan, P. M., Nanotubes from carbon. *Chem. Rev.*, 1999, **99**, 1787–1799.
23. Bengisu, M., *Engineering Ceramics*. Springer-Verlag, Berlin, 2001 (Chapter 4), p. 227.
24. Anstis, G. R., Chantikul, P. and Marshall, D. B., A critical evaluation of indentation technique for measuring fracture toughness: I, direct crack method. *J. Am. Ceram. Soc.*, 1981, **64**, 533–538.
25. Chantikul, P., Anstis, G. R. and Marshall, D. B., A critical evaluation of indentation technique for measuring fracture toughness: II, strength method. *J. Am. Ceram. Soc.*, 1981, **64**, 539–543.
26. ASTM E399, Standard test method for plain strain fracture toughness of metallic materials. *Annual Book of ASTM Standards, V.03.01*. ASTM, Philadelphia, USA, 1991.
27. Shen, T. K. and Hing, P., Ultrasonic through-transmission method of evaluating the modulus of elasticity of Al_2O_3–ZrO_2 composite. *J. Mater. Sci.*, 1997, **32**, 6633–6638.
28. An, J. W. and Lim, D. S., Effect of carbon nanotube addition on the microstructure of hot-pressed alumina. *J. Ceram. Process. Res.*, 2002, **3**(3), 201–204.
29. Xia, Z. and Xu, J. M., Direct observation of toughening mechanism in carbon nanotube ceramics matrix composites. *Acta Mater.*, 2004, **52**, 931–944.
30. Quinn, G. D. and Bradt, R. C., On the Vickers indentation fracture toughness test. *J. Am. Ceram. Soc.*, 2007, **90**(3), 673–680.
31. Kim, B. N., Wakayama, S. and Kawahara, M., Characterization of 2-dimesional crack propagation behaviour simulation and analysis. *Int. J. Fracture*, 1996, **75**, 247–259.
32. Ajayan, P. M. and Ebbesen, T. W., Nanometre-size tubes of carbon. *Rep. Prog. Phys.*, 1997, **60**, 1025–1062.
33. Thostenson, E. T., Ren, Z. and Chao, Advances in the science and technology of carbon nanotubes and their composites a review. *Comp. Sci. Technol.*, 2001, 899–1921.
34. Wichmann, M. H. G., Schulte, K. and Wagner, H. D., On nanocomposite toughness. *Comp. Sci. Technol.*, 2008, **68**, 329–331.
35. Ahmad, I., Kennedy, A. and Zhu, Y. Q., Interfacial investigations and mechanical properties of Carbon nanotube reinforced Al_2O_3 nanocomposites. In *Proceedings of the ICCM17: 17th International Conference on Composite Materials*, 2009.
36. Jinpeng, F., Zhuang, D. M. and Wu, M. S., Toughening and reinforcing alumina matrix composite with single walled carbon nanotubes. *Appl. Phys. Lett.*, 2006, **89**, 121910.
37. Flahaut, E., Peigney, A. and Rousset, A., Carbon nanotube-metal-oxide nanocomposite: microstructure, electrical conductivity and mechanical properties. *Acta. Mater.*, 2000, **48**, 3803–3812.